ARMY RESEARCH LABORATORY

Dynamic Multiaxial Response of a Hot-Pressed Aluminum Nitride

by Guangli Hu, C. Q. Chen, K. T. Ramesh, and J. W. McCauley

ARL-RP-0487 **June 2014**

A reprint from *Scripta Materialia*, Vol. 66, pp. 527–530, 2012.

NOTICES

Disclaimers

The findings in this report are not to be construed as an official Department of the Army position unless so designated by other authorized documents.

Citation of manufacturer's or trade names does not constitute an official endorsement or approval of the use thereof.

Destroy this report when it is no longer needed. Do not return it to the originator.

Army Research Laboratory
Aberdeen Proving Ground, MD 21005-5066

ARL-RP-0487 **June 2014**

Dynamic Multiaxial Response of a Hot-Pressed Aluminum Nitride

Guangli Hu, C. Q. Chen, and K. T. Ramesh
Johns Hopkins University

J. W. McCauley
Weapons and Materials Research Directorate, ARL

A reprint from *Scripta Materialia*, Vol. 66, pp. 527–530, 2012.

REPORT DOCUMENTATION PAGE

Form Approved
OMB No. 0704-0188

1. REPORT DATE *(DD-MM-YYYY)*	2. REPORT TYPE	3. DATES COVERED (From - To)
June 2014	Reprint	January 2010–January 2013

4. TITLE AND SUBTITLE
Dynamic Multiaxial Response of a Hot-Pressed Aluminum Nitride

5a. CONTRACT NUMBER

5b. GRANT NUMBER

5c. PROGRAM ELEMENT NUMBER

6. AUTHOR(S)
Guangli Hu, C. Q. Chen, K. T. Ramesh, and J. W. McCauley

5d. PROJECT NUMBER

5e. TASK NUMBER

5f. WORK UNIT NUMBER

7. PERFORMING ORGANIZATION NAME(S) AND ADDRESS(ES)
U.S. Army Research Laboratory
ATTN: RDRL-WM-OD
Aberdeen Proving Ground, MD 21005-5066

8. PERFORMING ORGANIZATION REPORT NUMBER
ARL-RP-0487

9. SPONSORING/MONITORING AGENCY NAME(S) AND ADDRESS(ES)

10. SPONSOR/MONITOR'S ACRONYM(S)

11. SPONSOR/MONITOR'S REPORT NUMBER(S)

12. DISTRIBUTION/AVAILABILITY STATEMENT
Approved for public release; distribution is unlimited.

13. SUPPLEMENTARY NOTES
A reprint from *Scripta Materialia*, Vol. 66, pp. 527–530, 2012.

14. ABSTRACT
The dynamic multiaxial response of hot-pressed AlN is characterized through quasi-static uniaxial compression, dynamic uniaxial compression and dynamic confined compression experiments within the strain rate range of 10^{-3}–10^{3} s^{-1}. Real-time visualization shows the failure patterns change from axial splitting under uniaxial dynamic compression to shear faulting under confinement. The compressive strength is moderately sensitive to both the confining stress and the loading rate. Post-mortem fracture surface studies show that the dominant fracture mechanism remains transgranular fracture under all loading conditions.

15. SUBJECT TERMS
aluminum nitride, dynamic testing, compression test, ceramics, strain rate, fracture

16. SECURITY CLASSIFICATION OF:			17. LIMITATION OF ABSTRACT	18. NUMBER OF PAGES	19a. NAME OF RESPONSIBLE PERSON
a. REPORT	b. ABSTRACT	c. THIS PAGE			J. W. McCauley
Unclassified	Unclassified	Unclassified	UU	10	19b. TELEPHONE NUMBER (*Include area code*) 410-306-0711

Standard Form 298 (Rev. 8/98)
Prescribed by ANSI Std. Z39.18

Available online at www.sciencedirect.com

SciVerse ScienceDirect

Scripta Materialia 66 (2012) 527–530

Scripta MATERIALIA

www.elsevier.com/locate/scriptamat

Dynamic multiaxial response of a hot-pressed aluminum nitride

Guangli Hu,[a,*] C.Q. Chen,[a] K.T. Ramesh[a] and J.W. McCauley[b]

[a]*Department of Mechanical Engineering, Johns Hopkins University, Baltimore, MD 21218, USA*
[b]*US Army Research Laboratory, Aberdeen Proving Ground, MD 21078, USA*

Received 14 December 2011; accepted 24 December 2011
Available online 5 January 2012

The dynamic multiaxial response of hot-pressed AlN is characterized through quasi-static uniaxial compression, dynamic uniaxial compression and dynamic confined compression experiments within the strain rate range of 10^{-3}–10^{3} s^{-1}. Real-time visualization shows the failure patterns change from axial splitting under uniaxial dynamic compression to shear faulting under confinement. The compressive strength is moderately sensitive to both the confining stress and the loading rate. Post-mortem fracture surface studies show that the dominant fracture mechanism remains transgranular fracture under all loading conditions.

Keywords: Compression test; Ceramics; Strain rate; Fracture; Confining stress

Aluminum nitride (AlN), in the commonly found wurtzite structure, is in the 6 mm point group, with lattice parameters of $a = 0.311$ nm, $c = 0.498$ nm and $c/a = 1.6$ [1]. This material has been widely used in electronic packaging due to its large band gap (6.2 eV), low thermal expansion, high thermal conductivity (200 W mK^{-1}) and high melting point [2]. It has also been considered as a potential armor material because of its low mass density (~3.26 g cm^{-3}), high hardness (~11.4 GPa [3]), relatively high Hugoniot elastic limit (~9 GPa [4,5]) and plastic deformation under confined conditions [6–9]. Further, some ballistics tests have suggested that AlN is a good performer under high impact velocities when compared to alumina, boron carbide, silicon carbide and titanium diboride [10].

There are two common approaches to the production of bulk polycrystalline aluminum nitride tiles: liquid phase pressureless sintering ("sintered AlN") and hot pressing ("hot-pressed AlN"). Sintered AlN generally contains a second phase, the sintering aid, which is added during the manufacturing process to provide rapid densification without the need for any external pressure [11], while a smaller amount of a sintering aid is added during hot pressing, which requires external pressure during the compaction process. These two manufacturing process can lead to very different initial defect structures inside the material, resulting in varied mechanical responses.

Over the past decade, several studies have been conducted to understand the mechanical response of AlN. This response has been studied through quasi-static uniaxial compression for both sintered and hot-pressed AlN [3,6,7,12], quasi-static triaxial compression for hot-pressed AlN [6], dynamic uniaxial compression for both sintered and hot-pressed AlN [3,7,12], dynamic triaxial confined compression at moderate confining pressures (less than 230 MPa) for sintered AlN [12], dynamic planar confinement experiments for sintered AlN [7], and plate impact experiments for hot-pressed AlN [13–15]. However, there is little confined dynamic work on hot-pressed AlN with a confining stress higher than 0.5 GPa. Confined dynamic experiments are of great interest because they provide a way to study mechanical response under the high strain rates and multiaxial stress states that develop in impact events. Further, few have explored the fracture mechanisms of hot-pressed AlN under different loading conditions [3], which is closely tied to the multiaxial mechanical response.

In this study, hot-pressed AlN samples were subjected to uniaxial quasi-static compression, uniaxial dynamic compression and confined dynamic compression, with high-speed real-time visualization in the latter two conditions. Post-mortem scanning electron microscopy (SEM) analysis was then used to study the fracture mechanisms that operated under the different loading conditions.

* Corresponding author. Tel.: +1 410 516 4398; fax: +1 410 516 7254; e-mail: ghu6@jhu.edu

1359-6462/$ - see front matter © 2011 Acta Materialia Inc. Published by Elsevier Ltd. All rights reserved.
doi:10.1016/j.scriptamat.2011.12.037

Hot-pressed AlN tile, with an average grain size of 4 μm, was provided by CoorsTek Vista. Figure 1(a) shows a representative transmission electron microscopy (TEM) micrograph of the as-received hot-pressed AlN, demonstrating no second phases along the grain boundaries or at triple junctions. For comparison purposes, Figure 1(b) shows a typical TEM micrograph of the as-received sintered AlN [7] provided by Dow Chemical, demonstrating that a number of the grain boundaries and triple junctions are occupied by second phases. These microstructural differences contribute to the different mechanical responses and corresponding fracture mechanisms between these two materials, as will be discussed next. The theoretical density of hot-pressed AlN is 3.26 g cm^{-3} and the measured density is 3.24 g cm^{-3}, giving a measured density to theoretical density ratio of 0.994. Cuboid samples were machined from the as-received material, resulting in sample dimensions of 3.5 mm × 4.0 mm × 5.3 mm, with the loading direction along the 5.3 mm axis. The parallelism tolerance of the loading surface was within 3 μm.

The rest of this manuscript focuses on the results on this hot-pressed AlN. Detailed descriptions of all the experimental techniques can be found elsewhere [7].

Quasi-static uniaxial compression experiments were conducted at a nominal strain rate of 10^{-3} s^{-1} on a servo-hydraulic MTS machine. Compressive strength is defined as the peak stress that is sustained by the specimen during the controlled rate experiments. The average compressive strength is about 2.6 GPa and images captured during the tests indicate crack growth is mainly along the principal compressive loading direction, consistent with the classical wing-crack model [16,17].

Dynamic uniaxial compression experiments were conducted on a Kolsky bar [7]. The stress history with high-speed photographs is not shown. The nominal strain rate is of the order of 10^3 s^{-1}, six orders of magnitude greater than that under quasi-static compression. The failures are generally initiated at the corners, then horizontal cracks are formed and cross the whole sample along the loading direction, leading to axial splitting, similar to that of sintered AlN under dynamic uniaxial compression [7]. The velocity of the horizontal crack in hot-pressed AlN is of the order of 2500 m s^{-1}, while the Rayleigh wave speed in this material is 5820 m s^{-1} (i.e. the cracks are moving at $\geqslant \sim 0.43 c_R$). This observed crack velocity is larger than that observed in sintered AlN (~1500 m s^{-1} [7]). The development of axial cracks has been widely modeled through the wing-crack mechanism, and it is known that the growth dynamics has a strong effect on the compressive strength and strain rate sensitivity under uniaxial stress loading [18,19]. After the compressive strength is reached, substantial lateral dilation due to axial crack opening is also observed. The cracks interact and coalesce to form fragments, some of which are so fine that they form a powder.

A comparison of our results on the compressive strength of this hot-pressed AlN (normalized by the average quasi-static strength) as a function of log strain rate is presented in Figure 2, together with the data available in the literature [3,7,12]. Like many other ceramics [19–23], our results show an increase in strength when deformed at strain rates above 10^2 s^{-1}, although our results show a smaller increase. This rate dependence has been addressed through several models [18,19,24–27], most of which appeal the inertia associated with dynamic crack growth. Note that care must be taken into account for experimental artifacts [28,29].

Figure 2 also shows that the strength-rate dependences of AlN from different sources are different. This is likely due to the different microstructural internal defects, such as grain boundaries, triple junctions, second phases, pores and inclusions, associated with the different manufacturing processes. The rate-dependent behavior is intimately related to the pre-existing distribution of defects in ceramics, since they control the nucleation, growth and interaction of microcracks [18]. The density of the defects influences the apparent transition strain rate as well as the strengths that can be achieved. It is possible that our experiments here are all below the transition strain rate for this particular material.

Confined dynamic experiments were also conducted on a modified Kolsky bar by incorporating a pair of T-block-shaped fixtures to apply a confining stress. The confinement is applied along one principal axis of the cuboidal specimen and the dynamic loading direction is along a second principal axis, while the third principal direction is traction free to allow visualization of the real-time failure process [30]. Note that the confining stress is first applied in a quasi-static manner, and the dynamic compressive load is subsequently superimposed. A representative result of a dynamic confined experiment with a confining stress of 320 MPa and a nominal strain rate on the order of 10^{-3} s^{-1} on this hot-pressed AlN is presented in Figure 3. Both the stress history (stress along the dynamic loading direction) and

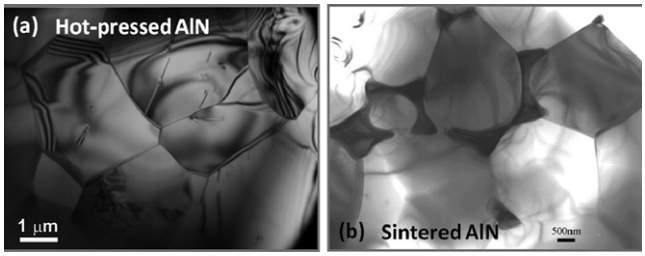

Figure 1. TEM micrographs of as-received (a) hot-pressed AlN and (b) sintered AlN.

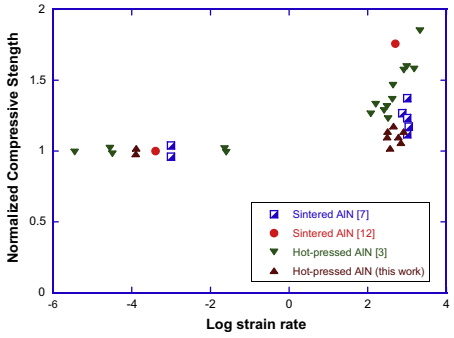

Figure 2. Normalized compressive strength of sintered AlN [7,12] and hot-pressed AlN ([3] and this work) as a function of log strain rate. The compressive strength is normalized by the average quasi-static strength of the corresponding material: sintered AlN [7], 3.2 GPa; sintered AlN [12], 2.5 GPa; hot-pressed AlN [3], 2.8 GPa; hot-pressed AlN, 2.6 GPa.

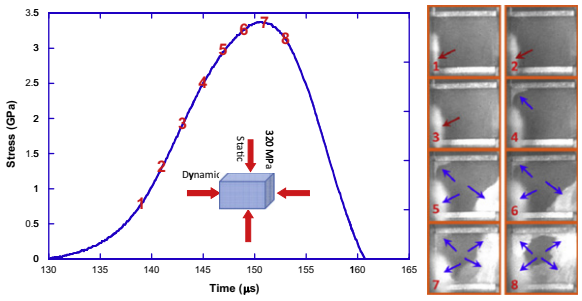

Figure 3. Stress history and high-speed camera images of confined dynamic compression with a confining stress of 320 MPa. (i) The inset shows the loading condition. (ii) The titanium alloy cushions (to evenly distribute the confining stress) can be clearly seen above and below the specimen in each frame.

the corresponding high-speed photographs are shown. The compressive strength is around 3.4 GPa, implying that confinement increases the strength. The high-speed photographs each have an exposure time of 350 ns, and the interframe time is 2 μs. These images show a significant change in the specimen failure process, in which no horizontal cracks are seen, but shear-dominated failure zones are observed in the specimen. The grey region (the red arrow) in the first three frames is believed to be the lubricant being squeezed out during the loading. An evident failure zone is first observed in frame 4, as indicated by the blue arrow, corresponding to a stress of about 2.5 GPa. With increasing loading, failure zones consecutively nucleate from all the corners till frame 7, which corresponds to the peak strength. The failure zone propagation direction is mainly along the shear direction instead of being aligned with the maximum principal loading direction. In frame 8, the failure zones coalesce with each other to form a continuous failure region. However, no horizontal cracks are observed in any of these frames, in contrast to the unconfined case. The presence of the confining stress appears to have dramatically changed the failure mode by suppressing the axial splitting and activating a shear-dominated failure mode. This failure mode transition was discussed in previous studies [7,12,17,31], but this is the first time that the shear-dominant failure pattern under confined dynamic loading condition has been visualized in situ. Similar shear-dominant failure patterns are also observed under a confining stress of 780 MPa.

The measured compressive strength of our dynamic confined experiments are plotted as a function of applied confining stress in Figure 4, along with the available

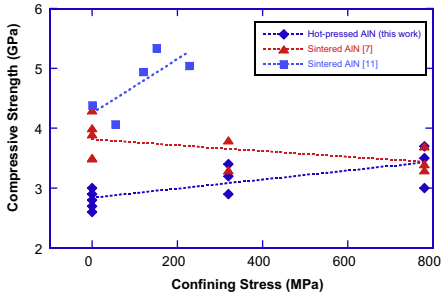

Figure 4. Confining stress effects under dynamic loading with a strain rate of $\sim 10^3\ s^{-1}$.

sintered AlN data that considers confinement [7,12]. The dashed lines are the linear fit of the data. Note that in the current study and in Hu et al. [7] the confined state is one of planar confinement, while Chen and Ravichandran [12] used a sleeve-based shrink-fit technique. Under the confined dynamic loading condition, our results for hot-pressed AlN show that the compressive strengths increase consistently with increasing confining stress. This increase in strength is likely because the confining stress suppresses the initiation/development of wing cracks (by decreasing the stress intensity factor at the wing-crack tip) [25,32]. We note that Chen and Ravichandran's [12] circumferential confinement data appear to be much more sensitivity to the confining stress than our planar confinement results. This can be explained by the difference in stress states between the two experimental techniques. Circumferential confinement corresponds to a triaxial stress state, while our planar confinement is essentially a biaxial stress state, having the possibility of stress relaxation due to lack of constraint along the direction of visualization. This stress relaxation perhaps results in the reduced sensitivity to the confining stress. Further, the planar confinement technique involves a different effect of the loading path on the mechanical response. The initial application of the confining stress can lead to the growth of some of the pre-existing defects in the material, so that the dynamic loading pulse perceives a material with a different defect distribution from the virgin material. Because of the globally compressive stress state, these cracks are typically of the wing-crack type, and have stress intensity factors that decrease with crack growth [16]; hence, the initial crack growth is stable. This weakening mechanism associated with the quasi-static preload and stress relaxation works against the hardening mechanism associated with the confinement, so we should not expect as much strengthening from the planar confinement experiment as would be expected from a triaxial experiment.

The results for sintered AlN [7] under dynamic planar confined loading are also plotted in Figure 4. Since these experiments were conducted using the same technique, we expect to see a slight increase in strength with confining stress. However, in contrast to the hot-pressed AlN, the compressive strength of sintered AlN appears to be insensitive to the confining stress, or even decreases slightly as the confining stress increases. We strongly believe that the different mechanical responses between the sintered and hot-pressed AlN under dynamic planar confined loading are due to the different initial defect distributions resulting from the manufacturing processes, as is partially shown in Figure 1.

Multiple fragments obtained after various experiments were examined by SEM to identify the fracture mechanisms. The fracture surfaces of fragments developed during uniaxial quasi-static ($\dot{\varepsilon} \sim 10^{-3} s^{-1}$) loading show primarily transgranular fracture, leaving a relatively smooth fracture surface. The competition between intergranular fracture and transgranular fracture is governed [33,34] by for transgranular fracture.

$$\frac{G_s^{Int}}{G_s^{Tra}} < \frac{\Gamma_C^{IT}}{\Gamma_C^{AlN}} \tag{1}$$

The quantities G_S^{Int} and G_S^{Tra} are the energy release rates of the intergranular and transgranular crack tips, while Γ_C^{IT} and Γ_C^{AlN} are the fracture toughnesses of the grain boundaries and the AlN grain. Compared to sintered AlN, hot-pressed AlN has no second phases along grain boundaries (as verified by SEM and TEM, Fig. 1), and it is quite possible that the grain boundary strength is comparable to the AlN grain strength. When the quasi-static toughness ratio between these two quantities is close to 1, the incoming crack tends to penetrate through the grains instead of kinking along the grain boundaries, resulting in transgranular fracture. However, there are some other materials, such as spinel [35], alumina [36] and sintered AlN [8], for which an intergranular failure mode was observed to be dominant under quasi-static loading. This is because these materials have either weak interfaces or second phases along the grain boundaries (which tend to be weaker than the grain itself [11]). In the current hot-pressed AlN, even under the quasi-static loading condition, the transgranular failure mode is dominant.

The typical fracture surfaces of fragments recovered after uniaxial dynamic compression (strain rates on the order of $10^3\ s^{-1}$) also show that the transgranular fracture mode is dominant. This observation agrees with experimental observations in another hot-pressed AlN system [3] and recent modeling work [37]. Under dynamic loading, the fracture mechanism competition is governed by the competition between the dynamic fracture toughness ratio and the dynamic energy release rate of the grain boundaries and the grains, similar to Eq. (1), but all the terms are crack velocity dependent. The grain boundary interface toughness will generally increase as a function of crack velocity due to a microbranching mechanism along the grain boundary, while the toughness of the grain is generally independent of crack velocity below a critical crack speed [38]. Therefore, during dynamic loading, it is even harder for the crack to kink along the grain boundaries, making transgranular fracture the preferred fracture mode. This transgranular fracture-dominant mode under impact loading conditions has also been observed in Al_2O_3 and SiC_w/Al_2O_3 [39].

Finally, the typical fracture surfaces from the fragments recovered from confined dynamic experiments (with strain rates of the order of $10^3\ s^{-1}$, with 320 and 780 MPa confining stresses) are also transgranular fracture dominant. This suggests that the confining stress has little effect on the fracture mode for hot-pressed AlN, while it has a significant effect on the sintered AlN system (through the second phase) [8]. The competition between intergranular and transgranular fracture as functions of loading rate and confining stress has been discussed elsewhere [8].

This work was performed under the auspices of the Center for Advanced Metallic and Ceramic Systems at the Johns Hopkins University, supported by the Army Research Laboratory under the REDCOM-ACQ-CTR Cooperative Agreement No. W911NF-06-2-0006.

[1] M.F. Denanot, J. Rabier, J. Mater. Sci. 24 (1989) 1594.
[2] I. Yonenaga, T. Shima, M.H.F. Sluiter, Jpn. J. Appl. Phys. 41 (2002) 4620.
[3] G. Subhash, G. Ravichandran, J. Mater. Sci. 33 (1998) 1933.
[4] Z. Rosenberg, N.S. Brar, S.J. Bless, J. Appl. Phys. 70 (1991) 167.
[5] D.E. Grady, Mech. Mater. 29 (1998) 181.
[6] H. Heard, C. Cline, J. Mater. Sci. 15 (1980) 1889.
[7] G. Hu, K.T. Ramesh, B. Cao, J.W. McCauley, J. Mech. Phys. Solids 59 (2011) 1076.
[8] Guangli Hu, C. Q. Chen, K. T. Ramesh, J. W. McCauley. Mechanism of dynamic deformation and dynamic failure in aluminum nitride, Acta Materialia, under review.
[9] J.W. McCauley, T.E. Wilantewicz, Army Research Laboratory, ARL-RP-268, 2009.
[10] J.E. Reaugh, A.C. Holt, M.L. Welkins, B.J. Cunningham, B.L. Hord, A.S. Kusubov, Int. J. Impact Eng. 23 (1999) 771.
[11] R.M. German, Liquid Phase Sintering, Plenum Press, New York, 1985.
[12] W.N. Chen, G. Ravichandran, J. Am. Ceram. Soc. 79 (1996) 579.
[13] Z. Rosenberg et al., J. Appl. Phys. 14 (1981) 261.
[14] D.P. Dandekar, A. Abbate, J. Frankel, J. Appl. Phys. 76 (1994) 4077.
[15] M.E. Kipp, D.E. Grady, Shock Phase-Transformation and Release Properties of Aluminum Nitride, Journal de Physique IV 4 (C8) (1994) 249–256.
[16] M.F. Ashby, S.D. Hallam, Acta Metall. 34 (1986) 497.
[17] H. Horii, S. Nemat-Nasser, J. Geophys. Res. 90 (1985).
[18] B. Paliwal, K.T. Ramesh, J. Mech. Phys. Solids 56 (2008) 896.
[19] B. Paliwal, K.T. Ramesh, Scr. Mater. 57 (2007) 481.
[20] T. Jiao, Y.L. Li, K.T. Ramesh, A.A. Wereszczak, Int. J. Appl. Ceram. Technol. 1 (2004) 243.
[21] H. Wang, K.T. Ramesh, Acta Mater. 52 (2004) 355.
[22] B. Paliwal, K.T. Ramesh, J.W. McCauley, J. Am. Ceram. Soc. 89 (2006) 2128.
[23] J. Kimberley, K.T. Ramesh, Scr. Mater. 65 (2011) 830.
[24] S. Nemat-Nasser, H. Deng, Acta Metall. 42 (1994) 1013.
[25] C.Y. Huang, G. Subhash, J. Mech. Phys. Solids 51 (2003) 1089.
[26] G. Ravichandran, G. Subhash, Int. J. Solids Struct. 32 (1995) 2627.
[27] J. Kimberley, G. Hu, K.T. Ramesh, Proceedings of SEM Series, Springer, New York, 2011, p. 419.
[28] G. Ravichandran, G. Subhash, J. Am. Ceram. Soc. 77 (1994) 263.
[29] G. Subhash, G. Ravichandran, ASM Handbook Volume 8, Mechanical Testing and Evaluation (ASM International), Materials Park, OH, 2000, p. 8.
[30] B. Paliwal, K.T. Ramesh, J.W. McCauley, M. Chen, J. Am. Ceram. Soc. 91 (2008) 3619.
[31] W. Chen, G. Ravichandran, J. Mech. Phys. Solids 45 (1997) 1303.
[32] H. Horii, S. Nemat-Nasser, Philos. Trans. R. Soc. Lond. A 319 (1986).
[33] Z.S.J.W. Hutchinson, Adv. Appl. Mech. 29 (1992).
[34] H. Ming-Yuan, J.W. Hutchinson, Int. J. Solids Struct. 25 (1989) 1053.
[35] J. Salem, L. Ghosn, Int. J. Fract. 164 (2010) 319.
[36] K.-H. Yang, A.S. Kobayashi, J. Am. Ceram. Soc. 73 (1990) 2309.
[37] R.H. Kraft, J.F. Molinari, K.T. Ramesh, D.H. Warner, J. Mech. Phys. Solids 56 (2008) 2618.
[38] K. Ravi-Chandar, Dynamic Fracture, Elsevier, Austin, TX, 2004.
[39] W.-J. Yang, C.-T. Yu, A.S. Kobayashi, J. Am. Ceram. Soc. 74 (1991) 290.

1 (PDF) DEFENSE TECHNICAL INFORMATION CTR DTIC OCA

2 (PDF) DIRECTOR US ARMY RESEARCH LAB RDRL CIO LL IMAL HRA MAIL & RECORDS MGMT

1 (PDF) GOVT PRINTG OFC A MALHOTRA

1 (PDF) NATL INST OF STANDARDS &TECH G QUINN

1 (PDF) ASSOC DIR MTRLS & STRUCTURES OASD(R&E) WEAPONS SYS AT&L (ASDR&E) L SLOTER

1 (PDF) WASHINGTON ST UNIV INST OF SHOCK PHYSICS Y GUPTA

1 (PDF) COORS CERAMIC CO F ANDERSON

1 (PDF) SIMULA INC V KELSEY

1 (PDF) PM HBCT SFAE GCS HBCT S J ROWE

1 (PDF) COMMANDER US ARMY RSRCH OFC D STEPP

1 (PDF) NAVAL SURFACE WARFARE CTR CARDEROCK DIV R PETERSON

1 (PDF) LAWRENCE LIVERMORE NATL LAB J E REAUGH L282

1 (PDF) SANDIA NATL LAB E STRACK

1 (PDF) RUTGERS THE STATE UNIV OF NJ DEPT OF CRMCS & MATLS ENGRG R HABER

1 (PDF) THE UNIV OF TEXAS AT AUSTIN S BLESS

1 (PDF) COMMANDER US ARMY TACOM L PROKURAT FRANKS

4 (PDF) JOHNS HOPKINS UNIV DEPT OF MECH ENGRG K T RAMESH T W RIGHT L CHROHM-BRADY K HEMKER

1 (PDF) CERADYNE INC M NORMANDIA

68 (25 HC, 43 PDF) DIR USARL
RDRL DPW
R COATES
RDRL VTP
E CHIN
RDRL WM
P BAKER
S KARNA
J MCCAULEY (15 HC)
RDRL WML
M ZOLTOSKI
RDRL WML H
T FARRAND
L MAGNESS
J NEWILL
D SCHEFFLER
R SUMMERS
RDRL WMM
J BEATTY
R DOWDING
J ZABINSKI
RDRL WMM A
J SANDS
RDRL WMM B
G GAZONAS
RDRL WMM D
K CHO
R SQUILLACIOTI
RDRL WMM E
J LASALVIA
P PATEL (10 HC)
J P SINGH
RDRL WMP
S SCHOENFELD
RDRL WMP B
C HOPPEL
M SCHEIDLER
T WEERASOORIYA

RDRL WMP C
R BECKER
T BJERKE
J CLAYTON
D DANDEKAR
M GREENFIELD
S SEGLETES
W WALTERS
RDRL WMP D
T HAVEL
M KEELE
D KLEPONIS
H MEYER
J RUNYEON
RDRL WMP E
P BARTKOWSKI
M BURKINS
W GOOCH
D HACKBARTH
E HORWATH
T JONES